Volume and pressure dependence of ground-state and lattice-dynamical properties of BaF_2 from density-functional methods

K. Schmalzl*
Forschungszentrum Jülich, 52425 Jülich, Germany and Institut Laue-Langevin, F-38042 Grenoble Cedex 9, France
(Received 3 October 2006; published 23 January 2007)

We have performed an *ab initio* study of BaF_2 by employing different program packages. Ground-state and lattice-dynamical properties are obtained from *ab initio* density-functional theory within local-density approximation (LDA) and generalized-gradient approximation (GGA) employing pseudopotentials and plane-wave basis sets, the electronic properties also from full-potential LAPW+LMTO methods. The results for the lattice constant and the electronic gap energies agree well within the LDA and GGA. For the band structure we found a valence-band maximum in the Σ direction in contrast to previous works. From density-functional perturbation theory we have calculated the phonon properties. Phonon dispersion curves, elastic constants, high-frequency dielectric constant, and effective charges and their volume and pressure dependence are presented. From the calculation of the anharmonic process of thermal expansion a softening of the X_2' mode was found similar to that in CaF_2.

DOI: 10.1103/PhysRevB.75.014306 PACS number(s): 63.20.Dj, 62.20.Dc, 65.40.De, 63.20.Ry

I. INTRODUCTION

Despite or because of their simple structure fluorites exhibit interesting properties and find a wide range of applications. Fluorites like CaF_2 and BaF_2 are members of the simplest classes of superionic conductors with a transition to the superconducting state[1] at about $T_c=1420$ K and 1233 K and a melting temperature[1,2] of about $T_m=1690$ K and 1593 K (Ref. 1) for CaF_2 and BaF_2, respectively. The fast ion conduction[3] with conductivities of more than 100 $(\Omega m)^{-1}$ is approaching those of ionic melts above a diffuse transition T_c [whereas ordinary solids show[1] a conductivity at moderate temperatures of 10^{-6} $(\Omega\ m)^{-1}$]. This conductivity is associated[4] with a disorder of the anion sublattice and mobile defects at a temperature T_c well below the general melting at T_m, whereas the cation lattice remains stable.[5] A large thermal motion is thereby associated with the anions.[6]

CaF_2 is widely used as a crystalline lens material for precision VUV optics, and BaF_2 represents an alternative material. Further reduction of size in photolithography is limited by the cutoff wavelength of the UV transmission. A decreasing wavelength raises problems making lenses to focus the radiation. For VUV radiation the lens material of choice is CaF_2 and BaF_2, both being wide-band-gap insulators. For processing, fabrication, and application, knowledge of volume- and temperature-dependent effects inducing stress and strain in the material is important. The technological importance asks for a good theoretical characterization of the fluorites.

Thus a study of the temperature or pressure dependence of physical properties like the dielectric constant or refractive index of ionic crystals is useful in view of their optical applications. Because of its simple structure and strongly temperature-dependent effects, the fluorite system may serve as a model system for anharmonic calculations. The success of harmonic *ab initio* calculations is well known,[7] but comparison with experiments demands further quantities like pressure dependence, thermal expansion, phonon lifetimes, or the shift of frequencies with changing temperature. A full anharmonic treatment is not feasible yet, but one approach is the calculation within a sort of quasiharmonic approximation in which anharmonic effects are taken into account via the volume dependence of phonon frequencies, like performed, e.g., in Refs. 8 and 9 to study thermodynamic properties in simple monatomic systems.

In this paper, BaF_2 is studied as a model fluorite employing the methods of density-functional theory and density-functional perturbation theory. The results are compared with those of the previously investigated CaF_2.[10] The focus is put on volume- and pressure-dependent properties. With the study of the ground-state and lattice-dynamical properties we want to add to the understanding of the perfect crystal and the anharmonic effects of lattice expansion and compression. As fluorites show huge anharmonic effects (like in CaF_2),[10] one can discriminate the thermal-expansion effects from the other anharmonic processes of an experiment by a calculation of volume-dependent properties.

BaF_2 crystallizes at ambient pressure in the cubic fluorite structure ($Fm3m$) made up of three interpenetrating fcc lattices with three atoms in the unit cell with Ba at (0, 0, 0) and F at $\pm(\frac{1}{4},\frac{1}{4},\frac{1}{4})a$ (see Fig. 1), with a being the lattice constant.

Like CaF_2, BaF_2 undergoes a first-order phase transition at room temperature (RT) from the fcc structure to an ortho-

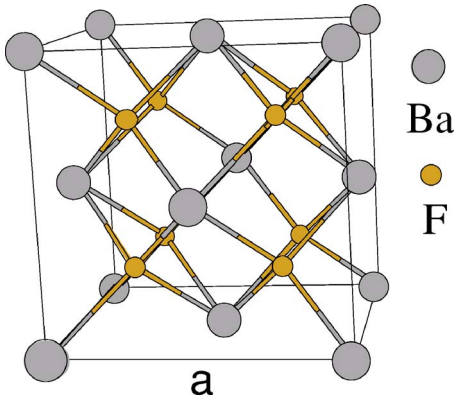

FIG. 1. (Color online) Crystal structure of BaF_2. The cube contains four formula units.

rhombic α-$PbCl_2$-like structure at high pressures. This transition occurs in CaF_2 at about 8 GPa (Ref. 11) and for BaF_2 somewhat lower at about 3 GPa (Refs. 12 and 13). With increasing pressure a second crystallographic transformation occurs to a hexagonal phase at about 12 GPa.[12,13] Metallization is found at about 33 GPa.[13] The frequencies of phonon modes increase with increasing pressure, and therefore also T_c increases.[14]

BaF_2 shows ionic conductivity higher than that in CaF_2.[3] The idea exists that the sublattice disorder is more extended in BaF_2 than in CaF_2 close to T_m because of the different cation radius.[15] Defects, hopping, and strong lattice anharmonicity seem to be characteristic of superionic conductors.

II. *AB INITIO* METHODS

The calculations of the electronic and dynamical properties have been performed in the framework of density-functional theory (DFT) by employing different program packages within the local-density (LDA) and generalized-gradient (GGA) approximations. The pseudopotentials have been taken from the ABINIT[16] and VASP[17] databases.

The lattice-dynamics calculations have been done with the linear-response approach (see, e.g., Ref. 7), implemented in the ABINIT program.

The ABINIT code gives direct access to various response functions that are second derivatives of the total energy with respect to different perturbations like phonon displacements or a static homogeneous electric field. The physical properties connected with respect to these perturbations are the phonon dynamical matrices, the dielectric tensor, and the Born effective charges.

With changing the volume and in this way simulating the thermal-expansion and pressure dependence we have obtained different physical properties like volume-dependent phonon frequencies or the related mode-Grüneisen parameters and the volume dependence of the elastic constants as well as of the high-frequency dielectric constant and of the Born effective charges.

III. GROUND-STATE RESULTS

A. Numerical details with application to the lattice constant

For the sake of comparison and testing, the lattice parameter has been calculated with different program packages and pseudopotentials. The WIEN97[18] code is an all-electron code, while the other codes are based on *ab initio* pseudopotentials; e.g., the ABINIT and VASP codes employ plane-wave expansions.

Within ABINIT the calculations were done with the Hartwigsen-Goedecker-Hutter[19] (HGH) pseudopotential for the Ba and F atoms. Semicore electrons assure a correct electronic response, since in view of the application to phonon properties, Ba loses all its valence electrons and the core electrons should dynamically arrange themselves as a function of phonon modes, which would be impossible in a frozen-core approximation. With this pseudopotential static and dynamic properties are well reproduced (see Secs. III B and IV A). Although HGH pseudopotentials demand a higher energy cutoff than, e.g., Troullier-Martins[20] (TM) pseudopotentials, they proved to give better and more reliable results for fluorites.[10,21]

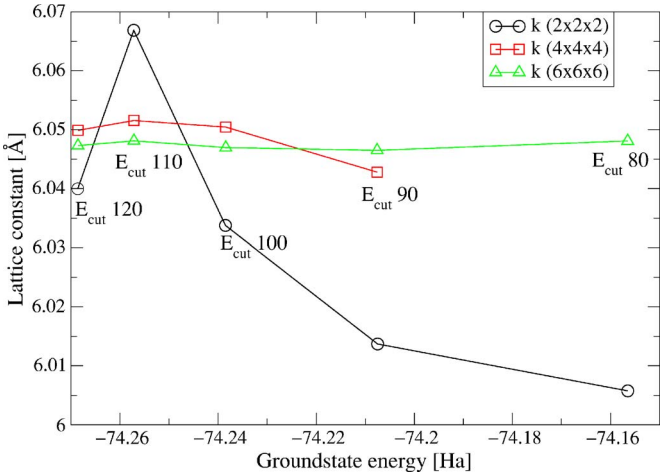

FIG. 2. (Color online) BaF_2: lattice constant (in Å) depending on the cutoff energy E_{cut} (in Ha) for various **k**-point meshes from ABINIT.

A Goedecker-Teter-Hutter[22] (GTH) or a TM pseudopotential for the F atom gives nearly no change in phonon frequencies, calculated for the HGH lattice constant, whereas a change of frequencies only in the range of 1%–2% is reached when a Teter (Te) pseudopotential for the Ba atom is employed, and a deviation of more than 20% in frequency appears when a TM pseudopotential for Ba is used, independent of the pseudopotential used for the F atom.

The lattice constant has been determined from the numerical minimum of the total energy. Figure 2 shows the convergence behavior of the ground-state lattice constant in the LDA for different **k**-point grids and as a function of the cutoff energy.

For the subsequent calculations we have chosen a $4\times4\times4$ special **k**-point grid and a cutoff energy of $E_{cut}=100$ Ha, resulting in $a=11.343a_{Bohr}=6.05$ Å.

In VASP a cutoff energy of 1000 eV has been used in the LDA, 1400 eV in the GGA, and a $4\times4\times4$ special **k**-point grid. In WIEN97 a dependence of the lattice constant upon the muffin-tin radius appeared in the 0.1% range. With increasing muffin-tin radius also the lattice constant becomes enlarged. In contrast to CaF_2 with nearly equal ionic radii of Ca and F, these are in a proportion of 1:1.3 in BaF_2. In the all-electron calculation a muffin-tin radius of $2a_{Bohr}$ for F and $2.4a_{Bohr}$ for Ba has been used.

The calculated lattice constants from different approaches and programs are listed in Table I together with other calculated and experimental values. The results of the different calculations in the LDA coincide quite well and likewise those in the GGA, but as already seen in CaF_2 and many other cases, the LDA underestimates the value of the experimental lattice parameter by a few percent and the GGA overestimates it. The calculation with CRYSTAL98, in which the method of linear combination of atomic orbitals (LCAO) is used, gives the largest lattice constant in the LDA as well as in the GGA, even if not as large as the Hartree-Fock (HF)

TABLE I. BaF_2: calculated and experimental lattice constants a (in Å). PW and PBE stand for the PW and PBE versions of the GGA.

Method	LDA	PW	PBE	Ref.
ABINIT (HGH)	6.05			Present
ABINIT (Te and TM)[a]	6.095	6.26		23
VASP (PAW)	6.094	6.279		Present
WIEN97	5.990	6.251	6.265	Present
WIEN97			6.233	24
(HSC)-Psp.	5.929			25
CRYSTAL98 (LCAO)		6.32		26
CRYSTAL98 (LCAO)	6.130	6.292		27
TB-LMTO	6.09			13
OLCAO	6.20			28
Expt. (300 K)	6.2			29
Expt. (300 K)	6.2			12
Expt. (295 K)	6.184			30

[a]Te for Ba, TM for F.

calculation[31] with $a=6.35$ Å. The calculation[25] with Hamann-Schlüter-Chiang[32] (HSC) pseudopotentials gives the smallest value, similar to CaF_2. VASP features the fastest performance but results in a relatively large lattice constant.

The deviation of the lattice parameter calculated in the LDA from the experimental one is similar to the one in CaF_2 ($a_{expt}=5.463$ Å, $a_{theor}=5.33$ Å), a bit more than 2%. Because of thermal-expansion effects, the theoretical lattice constant should be smaller than the room-temperature value. (The extrapolation of the experimental data to low temperatures should agree with the theoretical harmonic value.)

From the overall good agreement and the accordance between pseudopotential and all-electron methods the pseudopotentials used in the following seem reliable.

B. Electronic band structure

The electronic band structure and corresponding density of states have been calculated with WIEN97 and are shown in Fig. 3. The uppermost valence bands, shown here, originate from $2p$ states of the F atom. Further below, not shown here, are p states of Ba. The shown part of the conduction bands are d states of Ba, in agreement with experimental results and other calculations.[26,33] This is reasonable if one bears in mind that during the formation of ionic crystals electrons of the alkaline-earth atom are transferred to the p states of the halogen atom. Fully occupied p states of the anion dominate the valence band; the excited cationic states are in the conduction band.

Band-structure calculations for BaF_2 are rare, and the results are not quite clear. Our band structure as shown in Fig. 3 has been calculated within the LDA with similar results in the GGA. With the atoms in CaF_2 closer together than in BaF_2 the bands are narrower in the latter material: The valence band in BaF_2 is about half as wide as in CaF_2 and likewise the three-peak structure of the DOS originating from the first four states of the conduction band. Further

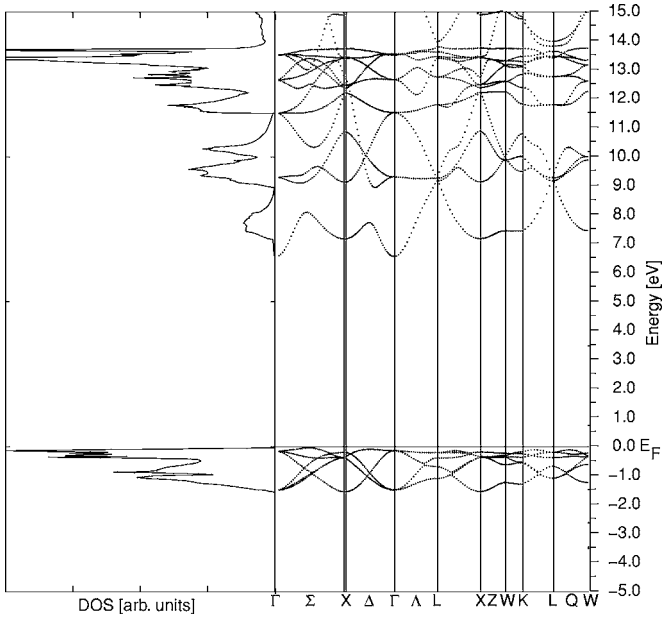

FIG. 3. BaF_2: electronic band structure (right) and corresponding density of states (DOS) (left) of the highest occupied and lowest unoccupied states from the FP-LAPW (WIEN97) calculation within LDA.

above, the band structures from different calculations differ from each other, like in CaF_2. For example, Ching *et al.*[28] found the upper valence band as nearly dispersionless.

The DOS of the valence band below the Fermi energy from tight-binding methods[34] is in good qualitative agreement with the one from this work; only the width of the band is smaller.

Like in CaF_2 we have obtained an indirect gap. The conduction-band minimum is at the Γ point, and the maximum of the valence band lies in the Σ direction near $\mathbf{q}=(\frac{1}{2},\frac{1}{2},0)$, while in CaF_2 it is at the X point. (In Ref. 24 the valence-band maximum was found in the Δ direction, probably only because the Σ direction was not investigated.) With decreasing lattice constant the gap energies increase. The gap energies are listed in Table II.

The experimental band-gap energy of about 10 eV is a bit smaller than that in CaF_2, where a gap between 11 and 12 eV resulted. The calculated values of the band gap do not deviate much from each other, but as is well known, in the LDA the gap is underestimated compared to experiment. From an LCAO method with CRYSTAL98, which is based on the Hartree-Fock method, the gap energy is overestimated by far ($\approx$20 eV) and results also in a qualitatively different band structure.[31]

IV. HARMONIC-PHONON RESULTS

A. Phonon dispersion curves

With three atoms in the unit cell of BaF_2 one expects nine branches. The transverse modes in the [001] and [111] direction are degenerate; no degeneracy exists along [110]. The lattice dynamics has been investigated by Hurrell and Minkiewicz[40] with inelastic neutron scattering at room tem-

TABLE II. Direct and indirect gap energies (in eV). The conduction-band minimum is generally at Γ, but in Ref. 28 it is found at *X*.

Method	Direct	Indirect	Ref.
WIEN97 (LDA)	6.7	7.197 (in Σ)	This work
WIEN97 (GGA-PW91)	7.197	7.097 (in Σ)	This work
WIEN97 (GGA)		6.97 (in Δ)	24
TB-LMTO (LDA)		7.033 (in *Z*)	13
TB-LMTO	6.37(?)	6.37(?)	35
DFT-LCAO	7.5		26
OLCAO (LDA)		7.19 (at *X*)	28
CRYSTAL98 (LCAO)	≈20		31
OPW	10.12		36
Reflection	11.0		36
Reflection (300 K)	11	10	37
Absorption (300 K)		9.06	38
Reflection and abs. (78 K)		10.59	39

perature for the main-symmetry directions [001] (Δ), [110] (Σ), and [111] (Λ). As in the measurements the $(1\bar{1}0)$ plane was used as the scattering plane, only six out of nine dispersion branches in the [110] direction are visible, the invisible branches (two Σ_3 and one Σ_2) being connected with ionic motion perpendicular to this plane. Figure 4 shows the measured together with the theoretical dispersion curves calculated with ABINIT and the corresponding one-phonon density of states.

For our calculations a cut off energy E_{cut} of 100 Ha and a special **k**-point mesh of $4\times4\times4$ have been used, as in the calculation of the lattice constant.

The results of Ref. 23 for the dispersion in the Δ and Σ directions show good qualitative agreement with ours, but because of their use of a $2\times2\times2$ **k**-point mesh, the optical modes deviate appreciably; in their coarse DOS, some of the main features are reproduced, but the tetrahedron method used in our case gives a much more detailed result.

TABLE III. BaF_2: theoretical and experimental optical Γ-point frequencies (in cm^{-1}).

Method	ω_{TO}	ω_{LO}	ω_{Raman}	Ref.
ABINIT	199.34	351.46	252.03	Present
ABINIT	≈200	≈349	≈257	23
IR, 80 K	189			41
IR, 4 K	193			42
IR refl., 5 K	190	346		43
IR refl., 300 K	187.5	344		43
IR refl., 300 K	184	326		44
Raman and IR, 300 K	189	330	241	45
Raman, 300 K		326	242	46

In Table III a comparison is made of our calculated Γ-point frequencies with some experimental values. The LO frequencies from infrared (IR) measurements were obtained from the Lyddane-Sachs-Teller (LST) relation[44] or from the Berreman technique[45] and compare reasonably well with each other and with other results. Also, reflectivity measurements[43] at low temperatures (5 K) together with a finding at 4 K cited in Ref. 42 resulted in higher frequencies and come closest to our calculated harmonic values as it should be.

A shell-model calculation of frequencies at the main symmetry points gives a maximum deviation of about 10% for lower frequencies and good agreement for higher frequencies.[47]

A comparison with the results for CaF_2 (Ref. 10) shows that because of the same fluorite structure, the branches result in a comparable picture. As the Ba atom is heavier than Ca, the one-phonon spectrum ranges in BaF_2 only up to 46 meV whereas in CaF_2 it extends up to 60 meV, and the elastic constants are smaller in BaF_2 as compared to those of

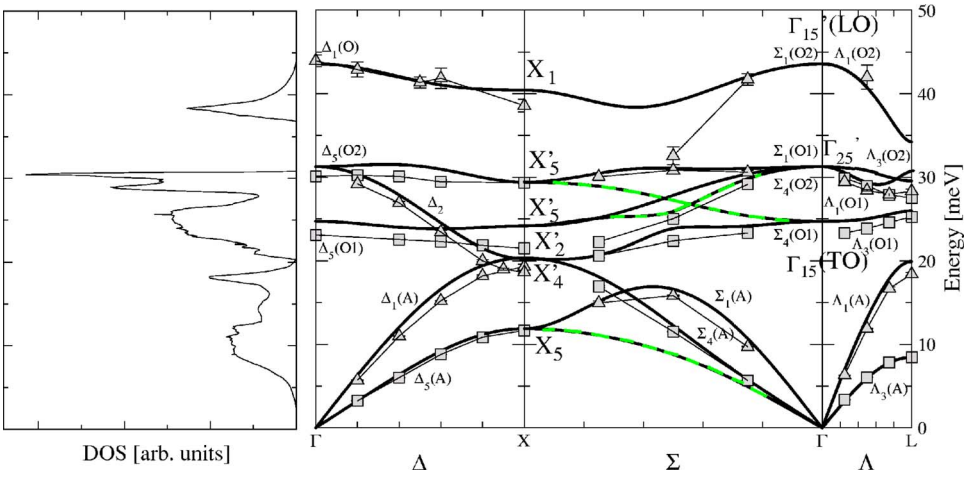

FIG. 4. (Color online) BaF_2: Right: phonon dispersion curves from inelastic neutron scattering (data points with thin connecting lines) at room temperature (Ref. 40) and from *ab initio* theory (thick lines). Triangles denote longitudinal, squares transverse polarization. The three lightly colored branches show modes which were not visible in the scattering geometry of the experiment. Left: phonon density of states from *ab initio* theory.

TABLE IV. BaF_2: calculated and experimental results for the elastic constants (in GPa). The present calculation was carried out for the theoretical lattice constant, $a=6.05$ Å. BS stands for Brillouin scattering; US stands for ultrasound technique with the 0 K data from extrapolation.

Method	c_{11}	c_{12}	c_{44}	Ref.
ABINIT	112.40	64.89	28.76	Present
HSC-Psp. (LDA)	110.33	54.33	27.4	25
CRYSTAL98 (LDA)	106.1	53.9	20.14	27
CRYSTAL98 (GGA)	92.6	40.2	21.78	27
WIEN97 (GGA)	90.14	39.53	25.02	24
Three-body shell-model	108.7	44.8	25.4	48
Three-body shell-model	109.2	39.8	23.2	49
Two-body shell-model	99.5	30.1	20.9	49
Rigid-ion model	98.21	25.90	31.30	50
Expt. 300 K	91.22	41.48	25.51	51
US (300 K)	89.15	40.02	25.35	52
US (0 K)	98.10	44.81	25.44	52
US (300 K)	92.06	≈42	25.68	53
US (300 K)	92.44	42.12	25.36	54
BS (300 K)	91.7	39.5	25.1	55

CaF_2 resulting in a smaller slope of the acoustic branches. Also, the optic branches show a lesser curvature. With the lattice constant calculated to be somewhat too small in the LDA, the theoretical frequencies are generally slightly too large, independent of the different pseudopotentials used.

Another difference is that the Δ_2 mode in BaF_2 is not the lowest frequency at the zone boundary (X_2') but meets the LA mode [$\Delta_1(A)$]. The highest mode along the Σ direction does not drop as much, like also shown in the shell-model calculation by Hurrell and Minkiewicz.[40] And at the L point a clear gap between the $\Lambda_3(O2)$ and $\Lambda_1(O2)$ modes shows up, because of lesser curvature of the $\Lambda_3(O2)$ modes, while in CaF_2 both modes could not be resolved. The theoretical results show good agreement with the experimental data of Hurrell and Minkiewicz[40]; minor deviations exist only at the L point, especially of the $\Lambda_3(O2)$ and $\Lambda_1(O1)$ modes.

B. Phonon eigenvectors

A look at the eigenvectors shows that in the Δ_2 modes only the F^- ions move whereas the Ba^{2+} or Ca^{2+} ions are at rest for the whole [100] direction. At the X point in this mode both F^- ions move parallel along a cube axis [100]. At the Γ point this is the threefold-degenerate Raman mode. The IR-active mode is LO-TO split. This splitting appears to be smaller in BaF_2 than in CaF_2 because of the larger reduced mass (see Sec. IV A).

In the X_1 mode both F^- ions move antiparallel, again along a cube axis. At the L point the F^- ions move parallel only in the $\Lambda_3(O1)$ and $\Lambda_1(O2)$ modes.

C. Elastic constants

A cubic crystal features three independent elastic constants, c_{11}, c_{12}, and c_{44}. The elastic constants have been obtained from the slopes of the acoustic branches along the three main-symmetry directions. The constants $c_{11}'=\frac{1}{2}(c_{11}+c_{12}+2c_{44})$ and $c'=\frac{1}{2}(c_{11}-c_{12})$ are the longitudinal and one of the shear constants for wave propagation along [110], the other being c_{44}.

Table IV shows calculated and experimental results for the elastic constants in BaF_2.

Our LDA calculations agree well with the findings from other methods using the LDA. However, the elastic constants are overestimated in the LDA calculations, particularly c_{12}, where one of the reasons is the theoretical lattice constant being smaller than the experimental one, see Table I.

Since the theoretical results for the elastic constants do not contain temperature effects, they should be compared to experimental low-temperature data. Extrapolation of the room-temperature data from the ultrasonic pulse-echo technique to $T=0$ K leads to values larger by about 10% for c_{11} and c_{12}, while c_{44} seems to remain rather constant.[52]

Neither in a rigid-ion nor in a shell-model can the elastic constants be reproduced properly; introduction of three-body interactions into a shell-model improves the fit.

V. RESULTS FOR THE PRESSURE AND VOLUME DEPENDENCE

A. Volume dependence of phonon frequencies

A homogeneous lattice contraction can be achieved with isotropic external pressure, while an expansion is usually due to thermal expansion. Actually, the latter effect is always accompanied by additional temperature-dependent anharmonic processes, to lowest order the two-phonon decay process and that of the coupling to thermal fluctuations. These latter effects can be treated only with explicit knowledge of the anharmonic coupling constants of third and fourth order, the calculation of which would be very much involved. However, the effect of homogeneous strain can be simulated simply by starting the computations from different lattice constants.

To lowest order of perturbation theory, the change of the lattice constants or of the (squared) phonon frequencies is proportional to the strain, and to lowest order the strain is proportional to the stress.

The first-order differentials of phonon properties have been calculated from differences taken for three different lattice constants $a=5.9$, 6.05, and 6.0 Å with $a=6.05$ Å being the relaxed lattice constant. In order to check for nonlinearities calculations have been performed for lattice constants in the range from $a=6.2$ to $a=6.8$ Å. (Actually, using thermal-expansion data of Ref. 56 melting occurs at an increase of the lattice constant of about 3%—i.e., near $a=6.2$ Å.)

As experimental results for the temperature-dependent dynamics for BaF_2 are not available (except for the modes with $\mathbf{q}=0$), a comparison is made mostly with theoretical results for the chemically and structurally related fluorite CaF_2.

1. Γ- and X-point modes

While in first-order perturbation theory the shift of the squared frequencies depends linearly on the change of the

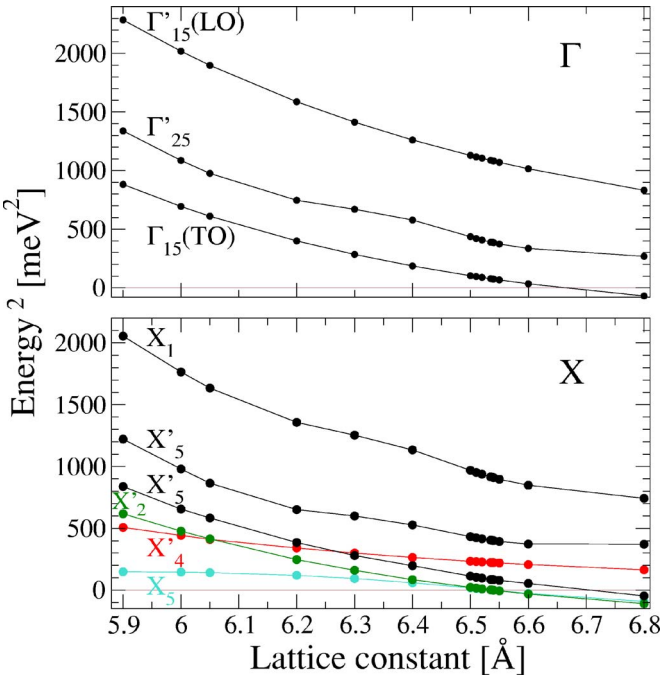

FIG. 5. (Color online) The theoretical volume dependence of the squared mode frequencies at the Γ and X points showing the (general and successive critical) softening of various modes as well as the nonlinear dependence. The X_2' mode, where only the F ions move and the acoustic X_5 and X_4' mode frequencies are plotted in different colors for clarity. The labels of the modes are the same as those in Fig. 4.

lattice constant a, the calculation of the frequencies for larger lattice-constant changes do show deviations from linearity.

Figure 5 shows the development of the squared Γ- and X-point frequencies with the change of the lattice constant. With increasing lattice constant Fig. 5 shows the expected decrease of all frequencies to lower energies. At first sight softening of various modes at the Γ as well as at the X point occurs. Well visible is the critical softening of the Γ_{15}(TO) mode [$\Delta_5(O1)$ branch] at $a \approx 6.6$ Å. At the X point one can see that the lowest transverse acoustic mode (X_5) becomes critically soft more or less simultaneously with the X_2' mode at $a \approx 6.54$ Å. Also the X_5' mode shows a zero crossing at an even larger value of a.

For lattice constants smaller than the equilibrium constant (corresponding to applied pressure) the X_2' mode frequency lies above the X_4' LA mode frequency. The near-degeneracy of these two modes, as shown in Fig. 4, seems to occur right at the equilibrium lattice constant $a=6.05$ Å. For hypothetical values $a > 6.4$ Å the X_5' TO mode frequency lies below the X_4' LA mode frequency.

A relatively small change of the lattice constant from $a=6.538$ Å to $a=6.540$ Å gives a barely visible change in frequencies except for the lowest zone-boundary (ZB) mode, where first the TA mode at the ZB becomes unstable between 6.538 and 6.539 Å, then the longitudinal X_2' mode between 6.539 and 6.54 Å.

Actually, the first unstable mode to occur upon expansion at 6.52 Å is an acoustic mode of mixed polarization in the Σ direction near the K point, $\mathbf{q}=(\frac{3}{4},\frac{3}{4},0)2\pi/a$, prior to any X mode instability.

At $a=6.55$ Å the transverse $\Delta_5(A)$ branch becomes imaginary, at $a=6.6$ Å the X_2' mode lies below the TA mode (X_5), and at $a=6.8$ Å the $\Delta_5(O1)$ and $\Lambda_3(O1)$ frequencies are imaginary.

With increasing lattice constant *all* modes at the X point soften in account of weakened forces (this is similar to the case of CaF_2). The rates of weakening of the lower-frequency modes differ from each other leading to various mode crossings. Critical softenings occur beyond melting (neglecting further anharmonic processes, which contribute to the phonon frequencies). This is different from the mode softening due to the double-well potentials in ferroelectrics, where the rate of weakening of the soft mode is *very* different from that of the other modes.

The slopes of the curves in Fig. 5 for BaF_2 are similar to the corresponding slopes in CaF_2 (see Fig. 12 in Ref. 10). This is a hint at the possibility that the anharmonicity is similar in these two systems and, consequently, that the behavior of the X-point modes in BaF_2 is properly described by just the anharmonic process of thermal expansion, while further phonon-phonon processes contribute to the temperature shift of the Γ-point frequencies.

Also similar is the deviation from the linear ω^2 vs a behavior because of further anharmonic contributions. Therefore, we believe that many conclusions concerning the anharmonic effects in BaF_2 can be taken from those in CaF_2.

2. X_2' mode

The displacement pattern of the X_2' mode describes out-of-phase moving neighboring chains of F^- ions in a rigid cation lattice. In BaF_2 and CaF_2 the X_2' mode becomes critically soft at nearly the same difference from the equilibrium lattice constant (0.43 in CaF_2 and 0.49 Å in BaF_2 and 0.3 and 0.34 Å in comparison to the experimental lattice constant). The critical softening of the X_2' mode indicates an instability of the lattice against building of a superstructure. However, melting seems to occur before critical softening.

Similar to our results, Makur and Ghosh[50] obtained with model calculations for BaF_2 a softening of the X_2' mode occurring *above* T_m and at higher temperatures than in CaF_2 where full softening is achieved below T_c (unlike in Ref. 10). Model potentials showed the softening of the X_2' mode at about T_c in CaF_2.[57,58] This softening was also found in calculation for SrF_2 (Ref. 59) and seems to constitute a specialty in fluorite systems, since it does not occur in normal ionic crystals like NaCl.[60]

The softening of the X_2' mode at increasing volume has been claimed to be connected to the transition to the superionic state of the fluorite system.[57,58] This softening is connected to reduced restoring forces acting on the displaced F^- ions. Then in the superionic phase there is a negligible resistance to perturbations of (collective) Δ_2-symmetry modes. But the reduced barriers may also support individual F^- hopping and may thus lead to more mobile anions.

This picture is also supported by neutron powder diffraction experiments[6] at high temperatures where the thermal motion of the anions is found to be much larger than that of the cations for $T \approx T_c$. Also, experimental anion mean-square displacements in fluorites like CaF_2 and BaF_2 are found to be

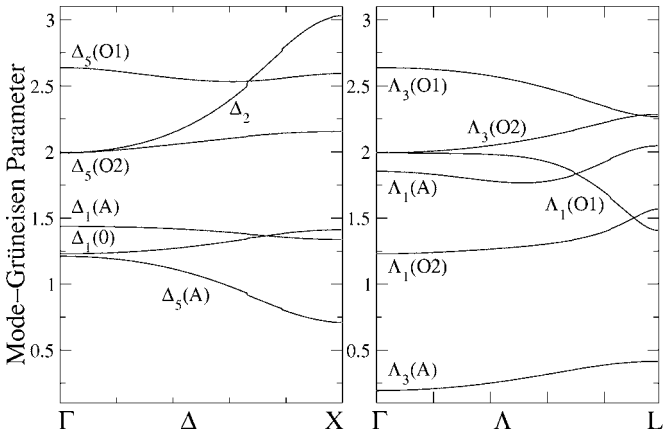

FIG. 6. BaF_2: theoretical wave vector dependence of the mode-Grüneisen parameters along the [001](Δ) and [111](Λ) directions. The labels of the branches of the dispersion curves are the same as those in Fig. 4.

much larger than the ones calculated in the quasiharmonic approximation for temperatures up to above T_c, suggesting a considerable anharmonicity or disorder in the anion sublattice.[61] This seems consistent with the large thermal expansion at T_c in both systems.

From quasielastic neutron scattering in, e.g., PbF_2 at higher temperatures (678 K) about 20% of the anions are displaced from their regular sites,[62] but since the anion Frenkel-pair generation in the fast-ion region is only about 10%,[63] not all F^- ions contribute to the superionic conduction. The diffusion and hopping occurring at higher temperatures have been modeled with a diffusion predominantly along the cubic axes and with clusters of anion Frenkel pairs consisting of interstitials, anion vacancies, and surrounding relaxed atoms.[64–66]

3. Mode-Grüneisen dispersion

While having looked so far only at the Γ- and *X*-point modes, we will now look at the other modes. In first-order perturbation theory the shift of the squared frequencies is proportional to the change of the lattice constant *a*. This relation is given by the mode-Grüneisen parameters

$$\gamma_\lambda = -\frac{d\ln\omega_\lambda}{d\ln V} = -\frac{1}{6}\frac{d\ln\omega_\lambda^2}{d\ln a}. \quad (1)$$

From the volume dependence of the frequencies we have calculated the mode-Grüneisen parameters (1) for BaF_2. Figure 6 shows the Grüneisen dispersion of all modes along the [001](Δ) and [111](Λ) directions.

A comparison to the Grüneisen dispersion of CaF_2 (see Ref. 10) shows a similar picture with some exceptions. Especially the Δ_2 modes exhibit the same striking behavior in BaF_2 as in CaF_2 and have the highest value at the ZB, even though a bit less in BaF_2 than in CaF_2. The branches $\Delta_5(O2)$, $\Delta_1(A)$, and $\Delta_1(O)$ show also the same tendency as in CaF_2 even if their slopes are bigger there. The modes $\Delta_5(A)$ and $\Delta_5(O1)$ show especially at the ZB a different behavior. In CaF_2, $\gamma_{\Delta_5(O1)}$ decreases at the ZB and $\gamma_{\Delta_5(A)}$ increases strongly; in BaF_2, both decrease slightly.

In the Δ direction, the range of parameters is comparable to that in CaF_2, but CaF_2 gives smaller values at the zone center, e.g., for the $\Delta_5(A)$ mode which starts at 0.75 in CaF_2 and at 1.21 in BaF_2. And in BaF_2 the $\Delta_5(A)$ mode shows a stronger curvature towards lower values.

In the Λ direction the modes $\Lambda_3(A)$, $\Lambda_3(O2)$, and $\Lambda_3(O1)$ result in a behavior similar to the one in CaF_2. Especially the modes $\Lambda_1(A)$ and $\Lambda_1(O1)$ in CaF_2 feature a stronger curvature towards the ZB. Also, the $\Lambda_1(O2)$ mode shows a positive slope here in contrast to CaF_2, where it is negative.

In summary, the Grüneisen parameters span a comparable range in both substances. The wave vector dependence of the parameters for the Δ and Λ direction shows a weaker curvature than in CaF_2, especially in the vicinity of the ZB.

From shell-model calculations, Ruppin[67] obtained a very similar mode-Grüneisen dispersion; only the labels $O1 \leftrightarrow O2$ have been interchanged.

TABLE V. BaF_2: theoretical and experimental optical Γ mode-Grüneisen parameters.

Method	TO	LO	Raman	Ref.
ABINIT	2.64	1.23	1.99	Present
Shell model	2.31	0.81	2.03	67
Mott-Littleton	2.67			68
Model	2.51	1.01		69
Expt.	2.4			43
Expt.		0.8		70
Expt.			1.8	71
Expt.			2.0	72
Expt.			1.78	73

4. Mode-Grüneisen parameters: LO, TO, and Raman modes

Experimental mode-Grüneisen parameters for TO and LO modes seem to be rare, while Raman data are somewhat more abundant. Available theoretical and experimental data of the mode-Grüneisen parameters of the optical Γ modes are collected in Table V.

Our *ab initio* values of the optical Γ mode-Grüneisen parameters seem to overestimate the experimental values. Other model calculations[74] give a wide range of values $1.36 < \gamma_{TO} < 2.84$ and $0.7 < \gamma_{LO} < 1.2$.

Assuming anharmonic effects other than that of thermal expansion to be negligible, we define an *effective* mode-Grüneisen parameter as

$$\tilde{\gamma}_\lambda = -\frac{1}{3\alpha_T}\frac{d\ln\omega_\lambda}{dT}, \quad \alpha_T = \frac{d\ln a}{dT}.$$

From temperature dependent data[43] and with the help of the coefficient of linear thermal expansion[56] $\alpha_T = 19.9 \times 10^{-6}\ K^{-1}$ at 300 K, we estimate $\tilde{\gamma}_{TO} = 2.0$ at RT, similar to the value for CaF_2, but slightly smaller than our value $\gamma_{TO} = 2.64$.

TABLE VI. BaF_2: theoretical and experimental long-wavelength acoustic mode-Grüneisen parameters for the main-symmetry direction. The parameters have been obtained from a quadratic interpolation of data at the lattice constants $a=6.0, 6.05, 6.2$ Å at $a=6.05$ Å.

	[001]		[111]		
Method	TA	LA	TA	LA	Ref.
ABINIT	1.211	1.436	0.194	1.853	Present
Expt.	0.69	1.32	−0.01	1.38	53
Expt.	0.6				77

The value $\tilde{\gamma}_{\text{Raman}}=1.36$ derived[75] from the temperature dependence is much smaller, and our estimate with the use of data from Ref. 76 gives a similar value ≈ 1.5.

The temperature dependence of the Raman mode is larger in BaF_2 than in CaF_2, while the pressure dependence of the Raman mode is about the same,[70] and that of the TO mode is smaller in BaF_2 than in CaF_2.

5. Mode-Grüneisen parameters: Long-wavelength acoustic modes

The mode-Grüneisen parameters of the long-wavelength acoustic modes have been obtained from the change of the dispersion-curve slopes with the change of volume. Present and experimental results are collected in Table VI.

While the experimental data for the TA[001] mode from ultrasound measurements[53] at 298 K and from thermal-expansion measurements[77] agree well, our theoretical value from the dispersion relation deviates rather strongly. A $6\times6\times6$ **k**-point mesh might improve the agreement. However, the mode-Grüneisen parameter for the TA mode in the [111] direction is clearly positive in our calculation.

6. Pressure dependence of the elastic constants

Because of the linear relation $\omega_{\mathbf{q}}=c_{\mathbf{q}}|\mathbf{q}|$ for the long-wavelength acoustic modes with the sound velocities $c_{\mathbf{q}}$ and since the $c_{\mathbf{q}}^2$ are proportional to linear combinations $f_{\mathbf{q}}(\{c_{ij}\})$ of the elastic constants c_{ij}, the mode-Grüneisen parameters can be written as

$$\gamma_{\mathbf{q}}=-\frac{d\ln\omega_{\mathbf{q}}}{d\ln V}=-\frac{1}{2}\frac{d\ln f_{\mathbf{q}}}{d\ln V},$$

characterizing the change of the elastic constants with the change in volume. In particular one has, e.g.,

$$\gamma_{\text{TA}[001]}=-\frac{1}{2}\frac{d\ln c_{44}}{d\ln V},\quad \gamma_{\text{LA}[001]}=-\frac{1}{2}\frac{d\ln c_{11}}{d\ln V}.$$

Assuming the relation $B=-(dp)/(d\ln V)$ with the bulk modulus $B=(c_{11}+2c_{12})/3$, the volume dependence of phonon frequencies or elastic constants can be converted into the pressure dependence,

$$\frac{d\ln c_{ij}}{dp}=-\frac{1}{B}\frac{d\ln c_{ij}}{d\ln V}. \tag{2}$$

These values are shown in Table VII and have been obtained from interpolation of data at the lattice constants $a=5.9, 6.0$ and $a=6.05$ Å. These values have been chosen to show the nonlinearity of the elastic constants under pressure. An analogous nonlinearity can be seen for the Γ- and X-point modes in Fig. 5. Otherwise the data in Tables VI and VII would be related to each other simply by the bulk modulus; see Eq. (2). For consistency we have taken the theoretical bulk modulus $B=89.8$ GPa. With somewhat too small a lattice constant, the force constants and thus elastic constants result in too large values, which amount to a factor of about 1.5 by which the bulk modulus is too large and the pressure dependence is too small. This, together with the deviations found in Sec. V A 5, should be taken into account when comparing the theoretical with the experimental values in Table VII.

The experimental data are in very good agreement, and if our theoretical data are multiplied by a factor of about 1.5 (correcting for the overestimated value of the bulk modulus) they would come much closer to the experimental values. Also, only small difference between theoretical and experimental values is to be expected, since upon cooling from

TABLE VII. BaF_2: calculated and experimental results for the logarithmic pressure derivative $(d\ln c_{ij})/(dp)$ of the elastic constants (in MPa^{-1}).

Method	$\frac{d\ln c_{11}}{dp}$	$\frac{d\ln c_{12}}{dp}$	$\frac{d\ln c_{44}}{dp}$	$\frac{d\ln c'}{dp}$	$\frac{d\ln c'_{11}}{dp}$
ABINIT[a]	34.6	58.3	19.1	−2.15	37.8
Ultrasound (300 K)[b]	52.7	124	30	−7.01	62.4
Ultrasound (300 K)[c]	52.4		30.3	−7.0	62.4

[a]This work.
[b]Reference 53.
[c]Reference 78.

TABLE VIII. BaF_2: calculated and experimental results for the effective charge Z^* and the high-frequency dielectric constant ϵ_∞.

Method	a[Å]	Z^*	ϵ_∞	Ref.
ABINIT (HGH)	6.05	2.634	2.472	Present
ABINIT (HGH)	6.2	2.585	2.398	Present
ABINIT	6.095	2.61		23
DFT-LCAO	6.32		2.012	26
OLCAO-LDA	6.2		1.12	28
LCAO-LDA (TDDFT)			1.97	79
WIEN97	6.233		2.129	24
CRYSTAL98	6.35	1.904		31
Bond orbital	6.21		2.15	in 80
Shell model	6.2		1.96	40
Model calc.		2.564		69
IR expt. (300 K)			2.16	44
Optical expt.			1.95	81
Expt. (300 K)			2.150	41
Expt. (4 K)			2.18	in 42
Expt. (300 K)	6.184		2.167	30

room to low temperature the pressure derivatives changes only by a few percent with a maximum change by about 10% in c' and c_{44}.[53]

The pressure derivative $(d \ln c')/(dp)$ is negative, as is $(d \ln c')/(dV)$, from theory and experiment in contrast to the other values. The relatively small modulus of it is also found in CaF_2.[53]

B. Volume dependence of the high-frequency dielectric constant and of the Born effective charges

In ionic crystals like the fluorites one has an LO-TO splitting. In BaF_2 at the Γ point there is a threefold-degenerate Raman-active mode near 31.25 meV and an infrared-active mode near 24.72 meV, where the LO mode experiences a huge LO-TO splitting given by

$$\omega_{\mathrm{LO}}^2 - \omega_{\mathrm{TO}}^2 = \frac{\mu}{V_0} \frac{(Z^* e)^2}{\epsilon_0 \epsilon_\infty},$$

with $\hbar\omega_{\mathrm{LO}}=43.576$ meV and $\hbar\omega_{\mathrm{TO}}=24.715$ meV. BaF_2 shows a similarly huge but slightly smaller splitting than CaF_2 (nearly 30 meV).

The Born effective charges are $Z^*=Z^*_{\mathrm{Ba}}=-2Z^*_{\mathrm{F}}$. Because of the cubic symmetry of the present system, the tensors of the dielectric constant and of the Born effective charges are diagonal.

The effective charges Z^* and the high-frequency dielectric constant ϵ_∞ have been calculated within the method of linear response. Table VIII lists various experimental and theoretical results.

1. Ground-state dielectric constant

The electrons of Ba are more extended and thus more polarizable than those in Ca resulting in a more polarizable system and in a higher dielectric constant. In general the high-frequency dielectric constant is believed to be overestimated by DFT in the LDA and GGA. The reason is seen in the underestimation of the band gap in LDA and GGA (see Sec. III B). Also our LDA calculation overestimates the value for ϵ_∞. The agreement with experiment becomes a bit better when the experimental lattice constant $a=6.2$ Å is used, see Table VIII or Fig. 8 below.

Inclusion of the so-called scissors operator changes the value from $\epsilon_\infty=1.12$ to $\epsilon_\infty=1.07$ (at $a=6.2$ Å).[28] *Ab initio* and deformation-shell model calculations result in values between 1.74 and 2.18.[82]

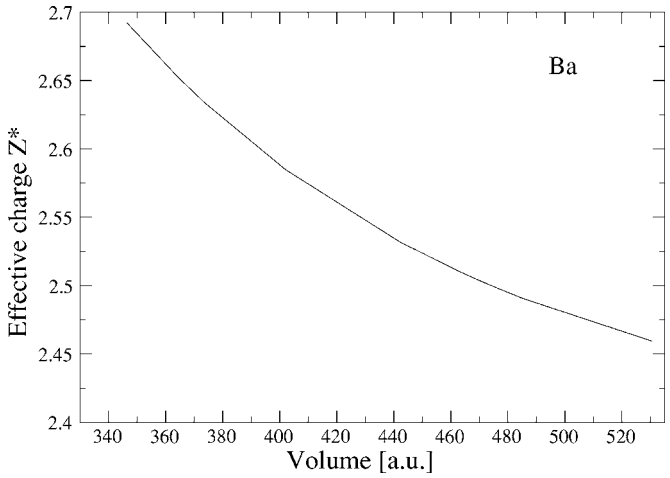

FIG. 7. BaF_2: theoretical volume dependence of the effective charge Z^* of the Ba^{2+} ion.

2. Ground-state effective charges

The effective charge of Ba is $Z^*=2.634$ at the theoretical ground state volume $V=374$ a.u. As in CaF_2 also in BaF_2 the effective charge is larger than the nominal ionic charge $Z_{\mathrm{Ba}}=2$. With the use of the experimental lattice constant, which is larger than the relaxed one, Z^* results in a somewhat smaller value.

3. Volume dependence

Both the high-frequency dielectric constant ϵ_∞ as well as the effective charge Z^* has been calculated within ABINIT for different volumes. The results are shown in Figs. 7 and 8.

At the theoretical equilibrium volume we find $(d \ln Z^*)/(d \ln V) \approx -0.25$, from pressure experiments[43] the value -0.3 is derived.

For the volume derivative of the dielectric constant we find $(d\epsilon_\infty)/(d \ln V)=-1.048$, in good agreement with -1.07 from Dutt *et al.*[69] Sharma and Shanker[83] obtained with electronic polarizabilities (Ruffa theory) a strain derivative of -1.15, somewhat larger than in CaF_2. A Penn-model calculation gives the wrong sign.[68]

As already seen in CaF_2, the dielectric constant as well as the effective charge shows a nonlinear volume dependence which indicates the importance of processes in perturbation theory beyond lowest order, in contrast to Ref. 24 where a linear dependence on pressure is claimed.

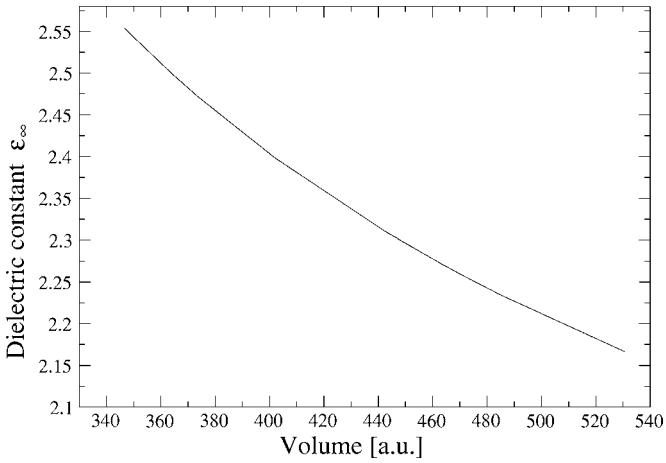

FIG. 8. BaF_2: theoretical volume dependence of the high-frequency dielectric constant ε_∞.

VI. CONCLUSIONS

We have presented a full *ab initio* study of the ground-state and vibrational properties of BaF_2 in generally good agreement with experimental and other theoretical data.

Due to the same crystal structure and due to nearly the same valence-electronic configuration of the Ba and Ca atoms, many findings are qualitatively similar to those encountered in CaF_2.

The electronic band structures of the two systems resemble each other. With the atoms in CaF_2 closer together than in BaF_2 the bands are narrower in the latter material. But there is a qualitative difference: The valence-band maximum of the electronic band structure of BaF_2 occurs in the Σ direction, while it is at the X point in CaF_2.

As in other materials, also the present lattice constant turns out to be smaller than the experimental one in the LDA and larger in the GGA. Consequently, the force constants, elastic constants, and phonon frequencies are somewhat too large in the LDA and too small in the GGA. Because of the mass of the Ba atom being larger than the Ca mass, the phonon frequencies in BaF_2 are generally smaller than those of CaF_2.

There are clear indications of a nonlinear volume and pressure dependence of all phonon properties. All modes soften upon expansion at a comparable rate (the rate being much smaller for the X_4' and X_5 modes) despite different irreducible representations, and a number of modes go soft at about a 10% increase of the equilibrium lattice constant. The mode-Grüneisen parameters of the Δ_1, Δ_2, $\Delta_5(O2)$, and Λ_3 modes behave similarly in BaF_2 and CaF_2, while there are quantitative and qualitative differences for the (transverse) $\Delta_5(A)$ and $\Delta_5(O1)$ and (longitudinal) Λ_1 modes.

Upon volume expansion, first the X_5 and then the X_2' mode go critically soft in BaF_2, while the order is reversed in CaF_2. Actually, the first mode to go soft is near the K point.

The Born effective charge $Z^* \approx 2.6$ of the Ba^{2+} ion is larger than the nominal ionic charge and even larger than that in CaF_2 ($Z^* \approx 2.4$).

ACKNOWLEDGMENT

The author thanks D. Strauch for numerous discussions and critical reading of the manuscript.

*Electronic address: schmalzl@ill.fr

[1] J. B. Boyce and B. A. Huberman, Phys. Rep. **51**, 189 (1979).
[2] B. F. Naylor, J. Am. Chem. Soc. **67**, 150 (1945).
[3] J. Oberschmidt and D. Lazarus, Phys. Rev. B **21**, 5823 (1980).
[4] J. Schoonman, in *Fast Ion Transport in Solids*, edited by P. Vanishta, J. N. Mundy, and G. K. Shenoy (Elsevier, Amsterdam, 1979), p. 631.
[5] M. H. Dickens, W. Hayes, C. Smith, M. T. Hutchings, and J. K. Kjems, in *Fast Ion Transport in Solids*, edited by P. Vanishta, J. N. Mundy, and G. K. Shenoy (Elsevier, Amsterdam, 1979), p. 229.
[6] M. W. Thomas, Chem. Phys. Lett. **40**, 111 (1976).
[7] S. Baroni, S. de Gironcoli, and A. Dal Corso, Rev. Mod. Phys. **73**, 515 (2001).
[8] A. Debernardi, M. Alouani, and H. Dreysse, Phys. Rev. B **63**, 064305 (2001).
[9] S. Narasimhan and S. de Gironcoli, Phys. Rev. B **65**, 064302 (2002).
[10] K. Schmalzl, D. Strauch, and H. Schober, Phys. Rev. B **68**, 144301 (2003).
[11] F. S. El'kin, O. B. Tsiok, L. G. Khvostantsev, and V. V. Brazhkin, JETP **100**, 971 (2005).
[12] J. M. Leger, J. Haines, A. Atouf, O. Schulte, and S. Hull, Phys. Rev. B **52**, 13247 (1995).
[13] V. Kanchana, G. Vaitheeswaran, and M. Rajagopalan, J. Alloys Compd. **359**, 66 (2003).
[14] A. E. Nikiforov, A. Y. Zakharov, V. A. Chernyshev, M. Y. Ougryumov, and S. V. Kotomanov, Phys. Solid State **44**, 1513 (2001).
[15] B. M. Voronin and S. V. Volkov, J. Phys. Chem. Solids **62**, 1349 (2001).
[16] X. Gonze, Phys. Rev. B **55**, 10337 (1997); see http://www.abinit.org
[17] G. Kresse and J. Furthmüller, Phys. Rev. B **54**, 11169 (1996); see http://cms.mpi.univie.ac.at/vasp/
[18] P. Blaha, K. Schwarz, P. Sorantin, and S. B. Trickey, Comput. Phys. Commun. **59**, 399 (1990).
[19] C. Hartwigsen, S. Goedecker, and J. Hutter, Phys. Rev. B **58**, 3641 (1998).
[20] N. Troullier and J. L. Martins, Phys. Rev. B **43**, 1993 (1991).
[21] M. Verstraete and X. Gonze, Phys. Rev. B **68**, 195123 (2003).
[22] S. Goedecker, M. Teter, and J. Hutter, Phys. Rev. B **54**, 1703 (1996).
[23] A. Dubinin, B. Winkler, K. Knorr, and V. Milman, Eur. Phys. J. B **39**, 27 (2004).
[24] R. Khenata, B. Daoudi, M. Sahnoun, H. Baltache, M. Rérat, A. H. Reshak, B. Bouhafs, H. Abid, and M. Driz, Eur. Phys. J. B **47**, 63 (2005).

[25] Z. H. Levine, J. H. Burnett, and E. L. Shirley, Phys. Rev. B **68**, 155120 (2003).
[26] H. Jiang, R. Pandey, C. Darrigan, and M. Rérat, J. Phys.: Condens. Matter **15**, 709 (2003).
[27] M. Mérawa, M. Llunell, R. Orlando, M. Gelize-Duvignau, and R. Dovesi, Chem. Phys. Lett. **368**, 7 (2003).
[28] W. Y. Ching, F. Gan, and M. Z. Huang, Phys. Rev. B **52**, 1596 (1995).
[29] R. W. G. Wyckoff, *Crystal Structures*, 2nd ed. (Wiley, New York, 1963), Vol. 1.
[30] G. A. Samara, Phys. Rev. B **13**, 4529 (1976).
[31] A. Y. Kuznetsov, A. B. Sobolev, A. N. Varaksin, J. Andriessen, and C. W. E. van Eijk, Phys. Solid State **45**, 838 (2003).
[32] D. R. Hamann, M. Schlüter, and C. Chiang, Phys. Rev. Lett. **43**, 1494 (1979).
[33] M. Itoh and H. Itoh, Phys. Rev. B **46**, 15509 (1992).
[34] E. Staritzky and L. B. Asprey, Anal. Chem. **29**, 856 (1957).
[35] V. P. Zhukov and V. M. Zaĭnullina, Phys. Solid State **40**, 1827 (1998).
[36] V. A. Ganin, M. G. Karin, V. K. Sidorin, K. K. Sidorin, N. V. Starostin, G. P. Startsev, and M. P. Shepilov, Sov. Phys. Solid State **16**, 2313 (1975).
[37] G. W. Rubloff, Phys. Rev. B **5**, 662 (1972).
[38] W. H. Strehlow and E. L Cook, J. Phys. Chem. Ref. Data **2**, 163 (1973), and references therein.
[39] T. Tomoiki and T. Miyata, J. Phys. Soc. Jpn. **27**, 658 (1969).
[40] J. P. Hurrell and V. J. Minkiewicz, Solid State Commun. **8**, 463 (1970).
[41] D. R. Bosomworth, Phys. Rev. **157**, 709 (1967).
[42] R. P. Lowndes, J. Phys. C **2**, 1595 (1969).
[43] R. P. Lowndes, J. Phys. C **4**, 3083 (1971).
[44] W. Kaiser, W. G. Spitzer, R. H. Kaiser, and L. E. Howarth, Phys. Rev. **127**, 1950 (1962).
[45] P. Denham, G. R. Field, P. L. R. Morse, and G. R. Wilkinson, Proc. R. Soc. London, Ser. A **317**, 55 (1970).
[46] R. Srivastava, H. V. Lauer, L. L. Chase, and W. E. Bron, Phys. Lett. **36A**, 333 (1971).
[47] N. Krishnamurthy and V. Soots, Can. J. Phys. **50**, 849 (1972).
[48] A. Basu, S. Sengupta, and A. N. Basu, Phys. Status Solidi B **103**, 535 (1981).
[49] S. Dasgupta, A. N. Basu, and A. Basu, Phys. Rev. B **30**, 7255 (1984).
[50] M. Makur and S. Ghosh, Phys. Status Solidi B **173**, 545 (1992).
[51] S. Haussühl, Phys. Status Solidi **3**, 1072 (1963).
[52] D. Gerlich, Phys. Rev. **135**, A1331 (1964).
[53] C. Wong and D. E. Schuele, J. Phys. Chem. Solids **29**, 1309 (1968).
[54] M. O. Manasreh and D. O. Pederson, Phys. Rev. B **31**, 3960 (1985).
[55] C. R. A. Catlow, J. D. Comins, F. A. Germano, R. T. Harley, and W. Hayes, J. Phys. C **11**, 3197 (1978).
[56] A. S. Touloukian, R. E. Kirby, R. E. Taylor, and T. Y. R. Lee, *Thermal Expansion: Nonmetallic Solids, Thermophysical Properties of Matter*, Vol. 13 (IFI/Plenum, New York, 1977).
[57] L. X. Zhou, J. R. Hardy, and H. Z. Cao, Solid State Commun. **98**, 341 (1996).
[58] L. L. Boyer, Phys. Rev. Lett. **45**, 1858 (1980).
[59] L. L. Boyer, Solid State Ionics **5**, 581 (1981).
[60] L. L. Boyer, Phys. Rev. Lett. **42**, 584 (1979).
[61] T. M. Haridasan, J. Govindarajan, M. A. H. Nerenberg, and P. W. M. Jacobs, J. Phys. C **15**, L93 (1982).
[62] K. Clausen, W. Hayes, M. T. Hutchings, J. K. Kjems, P. Schnabel, and C. Smith, Solid State Ionics **5**, 589 (1981).
[63] A. R. Allnatt, A. V. Chadwick, and P. W. M. Jacobs, Proc. R. Soc. London, Ser. A **410**, 385 (1986).
[64] M. T. Hutchings, K. Clausen, M. H. Dickens, W. Hayes, J. K. Kjems, P. G. Schnabel, and C. Smith, J. Phys. C **17**, 3903 (1984).
[65] G. Jacucci and A. Rahman, J. Chem. Phys. **69**, 4117 (1978).
[66] M. Dixon and M. J. Gillan, J. Phys. C **11**, L165 (1978).
[67] R. Ruppin, J. Phys. Chem. Solids **33**, 83 (1972).
[68] J. Shanker and R. Sundaraj, Phys. Status Solidi B **115**, 67 (1983).
[69] N. Dutt, G. G. Agrawal, and J. Shanker, Phys. Status Solidi B **131**, 505 (1985).
[70] J. R. Ferraro, H. Horan, and A. Quattrochi, J. Chem. Phys. **55**, 664 (1971).
[71] S. S. Mitra (unpublished), cited in Ref. 70.
[72] J. K. Kessler, E. Monberg, and M. Nicol, J. Chem. Phys. **60**, 5057 (1974).
[73] G. A. Kourouklis and E. Anastassakis, Phys. Status Solidi B **152**, 89 (1989).
[74] N. Dutt, A. J. Kaur, and J. Shanker, Phys. Status Solidi B **137**, 459 (1986).
[75] D. G. Mead and G. R. Wilkinson, J. Phys. C **10**, 1063 (1977).
[76] R. J. Elliott, W. Hayes, W. G. Kleppmann, A. J. Rushworth, and J. F. Ryan, Proc. R. Soc. London, Ser. A **360**, 317 (1978).
[77] G. K. White, J. Phys. C **13**, 4905 (1980).
[78] G. A. Samara, Phys. Rev. B **2**, 4194 (1970).
[79] F. Kootstra, P. L. deBoeij, and J. G. Snijders, Phys. Rev. B **62**, 7071 (2000).
[80] M. E. Lines, Phys. Rev. B **41**, 3372 (1990).
[81] I. H. Malitson, J. Opt. Soc. Am. **54**, 5 (1964).
[82] D. Kuhner and M. Wagner, Z. Phys. **256**, 22 (1972).
[83] J. C. Sharma and J. Shanker, Phys. Rev. B **19**, 6604 (1979).